11th International Conference on Fracture Mechanics of Concrete and Concrete Structures
FraMCoS-11
J. M. Chandra Kishen, A. Ramaswamy, S. Ray and R. Vidyasagar (Eds)
https://doi.org/10.21012/FC11.092323

A NOVEL EXPERIMENTAL METHOD TO CALCULATE THE FRACTURE SURFACE ENERGY OF GEOTHERMAL BEDROCKS IN REALISTIC TEMPERATURE CONDITIONS, AS A CONTRIBUTION TO CLIMATE CHANGE MITIGATION

OMAR RODRIGUEZ VILLARREAL [*], GILLES PIJAUDIER-CABOT, [*] CHRISTIAN LA BORDERIE, [*] ALBERTO VARELA [†] AND MOISES HINOJOSA RIVERA [†]

* Université de Pau et des Pays de l'Adour, E2S UPPA
SIAME and LFCR, Allée du Parc Montaury, 64600 Anglet, France
e-mail: edsciences@univ-pau.fr , www.univ-pau.fr

† Universidad Autónoma de Nuevo León
Facultad de Ingeniería Mecánica y Eléctrica,
Pedro de Alba s/n, Ciudad Universitaria, C.P 66451, Nuevo León, México
e-mail: contacto@fime.uanl.mx, https://www.uanl.mx/

Key words: Climate Change, Renewable Energy, Enhanced Geothermal Systems (EGS), Permeability, Hydraulic Fracturing, Fracture Energy.

Abstract: The challenges posed by climate change demand new advancements in fracture mechanics. In line with the Paris Agreement of 2015, one effective approach to mitigate greenhouse gas emissions is the utilization of renewable energy sources, including geothermal energy, coupled with continuous innovation and technological advancements. Geothermal energy remains an underutilized form of renewable energy, with the optimization of geothermal reservoirs relying on hydraulic fracturing to enhance permeability. To effectively carry out hydraulic fracturing, a thorough understanding of the fracture energy of the bedrock is essential. While experimental methods exist to measure fracture energy, the literature highlights certain limitations that have not been adequately addressed. An Enhanced Geothermal System (EGS) can be thought of as an underground heat exchanger designed to extract geothermal energy. The performance of these systems can be improved by increasing permeability with hydraulic fracturing, following the same technique used for hydrocarbon reservoirs. To understand hydraulic fracturing, whether it is implemented in an EGS or in a hydrocarbon reservoir, it is important to know the fracture parameters of the rock at stake, e.g., the fracture energy. We report here the use of a method based on an energy balance during hydraulic fracture tests. Specimens were prepared and they have been mechanically and hydromechanically characterized at 20 ºC and 100 ºC, a temperature representative of actual reservoir conditions. The fracture energy is obtained from a balance of kinetic, potential and pressure energies involved in the hydraulic fracture tests. The method provides fracture energies that are consistent with the literature data on similar materials. It is also found that the fracture energy increases upon heating.

1 INTRODUCTION

Human activities are exacerbating climate change, resulting in a significant rise in greenhouse gas emissions. In response to this pressing issue, the United Nations Framework Convention on Climate Change (UNFCCC) and the Paris Agreement 2015 advocate for emissions reduction through research and innovation in renewable energy sources. These efforts aim to mitigate climate change by regulating the production of greenhouse gases. This involves leveraging the potential of renewable energy options such as hydropower, solar power, wind energy, and geothermal energy [1-2]. The study "The Future of Geothermal Energy" by MIT suggests that Enhanced Geothermal Systems (EGS) are the future for geothermal energy utilization [3]. In the oil and gas industry, hydraulic fracturing has demonstrated its viability in the establishment of fracture networks in deposits with low permeability [4], this is also the case in the field of geothermal energy. A geothermal system can be thought of as an underground heat exchanger, and the surfaces where heat is exchanged with the circulating fluid should be as large as possible. This is the purpose of enhancement procedures based on hydraulic fracturing, yielding to an Enhanced Geothermal System (EGS).

Maximizing the surfaces where heat is exchanged means that the hydraulic fracturing process should be controlled as much as possible. Ideally, the induced fractures should be numerous, diffuse and connected to each other. Obviously, such a goal is difficult to achieve as rock properties, in situ stresses, and heterogeneities can neither be controlled nor changed. Nevertheless, a prerequisite for a better control, e.g., for hydraulic fracturing with multiple stages, is the knowledge of the fracture parameters of the rocks at stake [3]. Therefore, the estimation of the fracture energy (Gf), that is, the energy needed to create a fracture of unit surface, and its distribution in geothermal system need to be measured, or estimated, as accurately as possible. Geothermal reservoirs are made of different types of rocks such as granite, carbonate, and many others for which there exist reported values of fracture energy estimates [5]. An accurate determination of the fracture properties of rocks, however, relies on experimental testing methods and consistent interpretation models:

Extracting and machining fracture specimens according to standard procedures set, e.g., by ASTM (e.g., compact tension specimens) may not be feasible and in most cases only core-based specimens are available. Starting in the mid 80's the International Society for Rock Mechanics suggested several geometries for measuring the fracture toughness on core-based specimens [6-7]. Configurations include cylinder geometries and half-cylinder geometries subjected to bending, as well as disc geometries subjected to uniaxial compression.

Data interpretation is often based on linear elastic fracture mechanics (LEFM). However, in quasi-brittle materials such as rocks, concrete or mortars, the fracture resistance is increased by a hardening mechanism that originates at the tip of the crack, inside a region with non-linear behavior and distributed micro-cracking, the fracture process zone. The size of the fracture process zone does not depend on the size of the tested specimen and a size effect is observed [8], meaning that obtained the fracture energy and the apparent strength are size dependent. A size independent value of the fracture energy of the material can be derived from size effect tests [9]. For concrete, RILEM [10] developed such a standard procedure based of three point notched bending beams. For rocks, size effects are never considered in standards. It follows that the apparent fracture toughness that is usually obtained using LEFM is specimen-size dependent and overestimates the real material property generally [11]. The purpose of this paper is to present an experimental method that provides the estimation of the fracture energy directly from hydraulic fracture tests. Being based on energy conservation and on the area of the fracture created, it can be regarded as a method that easily provides the fracture properties of the tested material in the laboratory, without a mechanical model. Size effect is not accounted for here. Size effect

mechanical tests on rocks have been performed [12-13]. A size independent fracture energy could be obtained following our experimental methodology, at the price of experimental studies on specimens of various sizes.

The present technique may, in principle, also be implemented on site provided several conditions would be fulfilled: (1) the location of pre-existing fractures and the overall geometry of the reservoir should be known; (2) the site should be instrumented to determine the geometry of the hydraulically induced crack systems, e.g., with the localization of micro seismic events (similar to the analyses of acoustic emissions in laboratory tests); (3) upon crack propagation, micro-seismic analyses should provide a sufficiently accurate estimate of the generated crack surfaces. Would these conditions be met; the present method could provide estimates of the fracture energy of the horizon where the cracks propagate. In addition, site experiments might be considered as a possibility of avoiding the bias due to size effect, i.e., by measuring the fracture energy for the "real" geometry of the rock mass at stake.

The method discussed in this paper is developed at the laboratory scale. In the laboratory it is common to use synthetic rocks such as mortar and concrete to develop new experimental techniques [14-15]. For example, Mei et al. [16] has reported the successful use of synthetic rocks made of a mixture of cement, gypsum, sand, and water, and the validity of this approach has been recently reviewed [17]. We are going to follow the same idea here and consider first mortar specimens, then, fracture of limestone will be investigated. The experimental set-up allows the measurements of fracture energies at various temperatures. Fracture energies at 20º and 100º are reported, as these conditions are more representative of actual geothermal reservoir conditions. This paper is organized as follows: the experimental setup for hydraulic fracturing is presented in Sect. 2, along with material characterization according to standard procedures. We derive in Sect. 3 the fracture energy from conservation of energy considerations and discuss the results obtained on the mortar samples at room temperature. Section 4 presents the results obtained on limestone at two different temperatures: 20 º C and 100 º C.

In section 5, the conclusions are presented along with a QR code that provides access to an animated video. This video has been designed to effectively communicate our findings to a wider audience, aligning with the current trends of knowledge dissemination and social engagement.

2 HYDRAULIC FRACTURE TEST SET-UP AND CHARACTERIZATION

Hydraulic fracture tests are performed on hollow cylindrical specimens. Fluid is injected in the hollow cylinder under fixed fluid flow conditions and the pressure is increased until a maximum corresponding to the onset of fracture is reached. In the literature, several set-ups for performing hydraulic fracture tests can be found, mostly on prismatic specimens [18-19], but also on cylindrical specimens [20]. While tests on prismatic cylinders allow to apply lateral confinement stresses that are not equal, which is more representative of actual reservoir conditions, tests on cylinders are simpler to operate and may use a standard triaxial testing cell if the effect of triaxial states of stresses prior to fracture needs to be investigated. It is this type of geometry, placed in a uniaxial testing device that has been implemented in the present contribution. A schematic view of the testing device is shown in Fig. 1. Prior to describing these experiments, let us detail the specimen geometry and material characterization.

2.1 Preparation and Characterization

Cylindrical specimens with outer and inner diameter of 53 mm and 10 mm respectively, and height of 105 mm were fabricated. Mortar was prepared using CPC 30 R cement and fine aggregate with a maximum particle size of 1.40 mm and with a proportion of 1:2 and W/C ratio of 0.45, the specimens were cured during 28 days. The mortar specimens were dried following ASTM C-642 standard [21]. The

specimens were dried in a Vulcan 3-550 oven. They were heated at a rate of 1º C per minute from room temperature up to 100º C and maintained for four hours. Their dry mass (M_a), weight immersed in boiling water (M_w) and weight immersed in water (M_l) at room temperature were measured, then, the connected porosity of the material, denoted as, was evaluated following Eq. (1):

$$\phi = \frac{M_w - M_a}{M_w - M_l} \times 100. \quad (1)$$

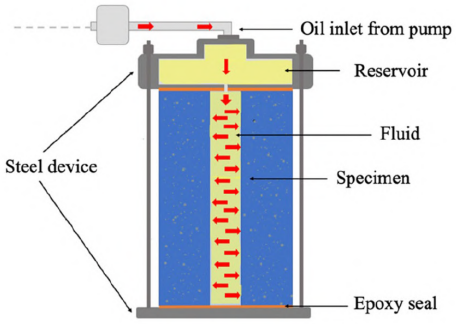

Fig.1 Testing set-up and cross-section of a typical specimen.

On average, the connected porosity was 14.07% for the mortar specimens. To measure their elastic properties and their compressive strength, the specimens were tested in uniaxial compression using a GCTS RTR 2000 triaxial machine. Subsequently, Brazilian tests were performed to obtain the tensile strength of mortar. Table 1 summarizes the results obtained on average for five samples for each test: The permeability was measured by injecting Mobil DTE 25 oil under pressure in the hollow cylinder with the help of a pump (Quizix model Q-5020-HC), as illustrated in Fig. 1. With the purpose of eliminating any humidity inside the specimens, they were dried following the same procedure as for the mechanical tests before starting the permeability tests. To avoid further contact with humidity, the specimens were placed in hermetic bags filled with Mobil DTE 25 oil. Then, the specimens were placed in the mechanical set-up (Fig. 2), a slight axial load of 525 N was applied to prevent leakage. Next, the fluid was injected at pressure levels of 600, 800, 1000, 1400 and 2000 kPa. The flow rate was measured upon reaching a steady state. The fluid flow rate was estimated by the PumpWorks software using the inner area of its cylinders and the speed of the pistons. For the calculation of the intrinsic permeability of mortar K, we assumed a radial flow in the hollow cylindrical specimen, from the inner surface of the specimen to its outer surface and used Darcy's law. Hence, the permeability reads:

$$K = \frac{Q\mu \ln\left({}^{b}/_{a}\right)}{2\pi H\left(p_i - p_e\right)}, \quad (2)$$

where Q is the measured flow rate (m^3/s), μ is the dynamic viscosity ($kN\text{-}s/m^2$), b the outer radius of the specimen, the inner radius, h the height of the specimen, p_i the inner pressure (kN/m^2) and p_e is the outer pressure (kN/m^2), i.e., the atmospheric pressure. The values of the dynamic viscosity of the fluid depends on temperature, as provided by the manufacturer. It is equal to 0.03872 $kN\text{-}s/m^2$ at room temperature and to 0.00587 $kN\text{-}s/m^2$ at 100º C according to ASTM D 445-06 standard. Figure 3 shows a typical plot of the fluid flow rate vs. the injection pressure.

Table 1: Mechanical characterization of mortar

Mechanical characterization	
Maximum compressive strength	29.78 ± 0.752 MPa
Young modulus	13.62 ± 0.397 GPa
Poisson ratio	0.15 ± 0.00548
Tensile strength	2.95 ± 0.110 MPa

Table 2: Permeability coefficient of the mortar

Mortar specimen	**Permeability coefficient (K, m^2)**
1	$0.98\text{x}10^{-18}$
2	$1.98\text{x}10^{-18}$
3	$5.93\text{x}10^{-18}$
4	$2.13\text{x}10^{-18}$
Average	$2.76\text{x}10^{-18}$

Table 2 presents the permeability results for the four mortar specimens. The dispersion among the measurements is typical of what could be expected in such tests. For instance, Choinska et al. [22] observed dispersion of the same order on the permeability of concrete measured with nitrogen using a similar apparatus. For mortar mixtures with a W/C ratio of 0.45 and 28 days of curing, permeability coefficients similar to those reported in this document have also been reported [23].

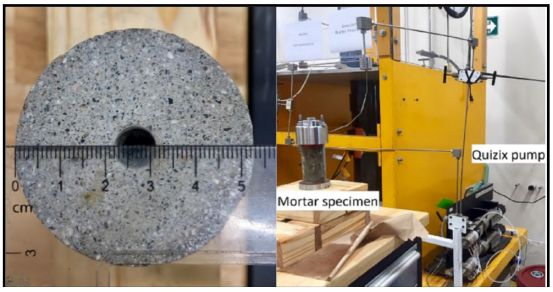

Fig. 2 Injection system for the permeability test

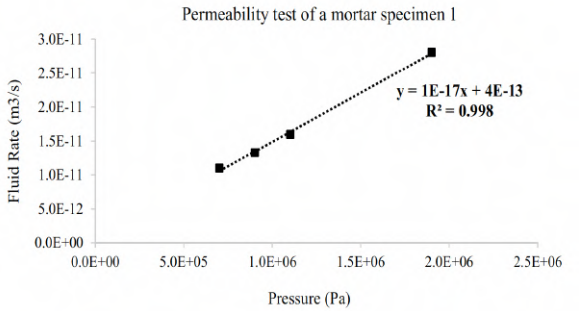

Fig. 3 Evolution of injected fluid flow rate as a function of the injection pressure in mortar specimen 1.

2.2 Hydraulic Fracture test

The hydraulic fracture tests were performed on the same specimens used for the permeability test and in the same device. The experiment consisted now in applying a constant flow rate of 0.05 mL/min of Mobile oil DTE 25 to the specimens after the permeability tests. The set-up is illustrated in Fig. 4. Figure 5 shows the records of the increase of pressure for the mortar specimens tested at ambient temperature. These curves are characterized by a relatively smooth increase of fluid pressure, followed by an abrupt drop down corresponding to the occurrence of fracturing. We may remark in this figure that there is one experiment where the pressure rises sooner compared to the others. Converted into a volume of injected fluid, the time difference (1000 s) corresponds to 0.8 ml which is very small. It may be due to a variation of the initial state of saturation in the specimen. This specimen might be better saturated prior to running the fracture experiment compared to the others. As we will see next, this discrepancy does not affect that much the interpretation of the test data which relies on the calculation of the integrals over time of these curves. The area under the curve in the initial regime, prior to the rise of pressure is very small compared to the area during the entire fracture process. This difference in the initial regime yields a dispersion on the fracture energy in the range of a few precents only (see Table 3). Figure 6 shows a specimen after the test has been completed. One can see the cracks that have been generated by the increase of pressure (two cracks that start from the borehole).

Table 3: Estimated fracture energy for the mortar specimens at room temperature

Mortar specimen	Fracture energy (J/m^2)
1	97.89
2	88.32
3	94.06
4	91.62
Average	92.97
Standard deviation	4.03

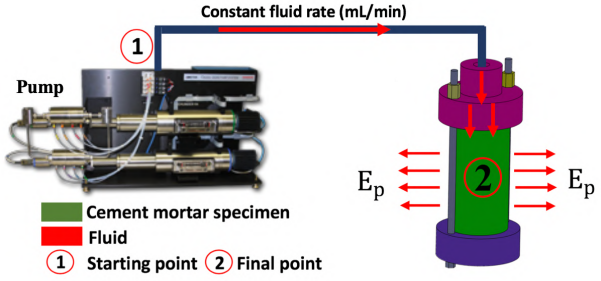

Fig. 4 Hydraulic fracture test system

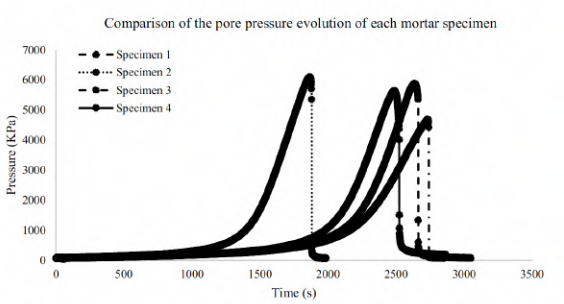

Fig. 5 Comparison of the inner pressure evolution of each mortar specimen tested at room temperature.

3 ESTIMATION OF FRACTURE ENERGY

To estimate the fracture energy, we consider the various energies at stake during the tests. We consider that the fluid is incompressible, with constant viscosity and constant density, and we apply Bernoulli's equation. During the hydraulic fracture tests carried out in the lab, the kinetic and potential energy (elevation of the fluid) of the fluid are small compared to the energy related to the pressurization of the fluid and their contributions are discarded (but should be accounted for in field applications). Therefore, the energy that is provided to the specimen originates mainly from the power supplied by from the pump to the fluid denoted as *W:*

$$W = (p_a A)(Q/A) = p_a \times Q, \tag{3}$$

where W is the power of the pump, pa is the fluid pressure in the inner hole of the mortar cylinder, Q is the fluid rate and A is the area of the cross section through which the fluid passes. Over a time, interval dt the energy provided by the pump is dE defined as:

$$\mathrm{d}E = W\mathrm{d}t. \tag{4}$$

Because the tests were carried out at a constant flow rate, the total amount of energy provided by the pump is:

$$E(t) = \int_0^t W\mathrm{d}t = Q\int_0^t p_a \mathrm{d}t, \tag{5}$$

Which means that this energy can be easily obtained by integrating the pressure histories in Fig. 5. According to the conservation of energy, the energy supplied by the pump over the entire hydraulic fracture process, at the end of the test corresponding to time t_f, must have been dissipated either due to the viscosity of the fluid E_μ, or due to the fracture of the specimen E_f:

$$E(t_f) = E_\mu + E_f \tag{6}$$

To isolate the energy consumed during the fracture of the specimen, we need now to estimate the dissipated energy due to viscosity, in other words, the dissipation due to Darcy's flow inside the specimen:

$$E_\mu = \int_0^{t_f} P(t) \times Q(t)\mathrm{d}t \tag{7}$$

where the pressure and fluid flow are now related by Darcy's law (Eq. 2). Over the specimen, Darcy's law translates into a linear relationship between the pressure and the fluid flow (which is set constant) as illustrated in Fig. 3. Therefore, this integral may be easily evaluated: for a typical fluid flow rate in the range of 0.1 mL/min, the integration over the test duration (2000–3000s) using the slope obtained in Fig. 3 yields an energy which is in the range of 0.01 J. Upon variations of temperature (e.g., from 20º to 100º C), the viscosity might change by an order of magnitude, but this energy will remain small. Compared to the energy that is expected to be dissipated during fracture, E_μ is negligible. Hence, the measured fracture energy does not depend on the properties of the pressuring fluid in the present case. It would not be the case if the dissipation of energy due to fluid flow in the various apparatuses or in the specimen due to Darcy flow is not negligible, or if the fluid would react with the rock. A correction of the energy balance would be needed to arrive to an intrinsic estimate of the fracture energy. In the present experiments, Eq. (6) provides the energy dissipated due to fracture as a function of the energy supplied by the pump. To obtain the fracture energy, we have now to divide E_f

by the area of fracture created during the test, A_f which will be obtained experimentally. Therefore:

$$G_f = \frac{Q \int_0^t p_a dt}{A_f}. \quad (8)$$

The fractured area created at the end of the hydraulic fracture test can be approximated as:

$$A_f = n(D_O - D_I)h, \quad (9)$$

where D_o and D_I are the outer and inner diameters of the specimen, respectively, h is the height of the specimen and n is the number of pieces the specimen is fractured into. All the specimens tested in this study were fractured in two parts and four fracture surfaces are generated (see e.g., Fig. 6), hence $n = 4$.

The estimate of the fracture energy, Eq. (8), has been used for the mortar specimens tested. The integrals of the pressure histories in Fig. 5 have been calculated according to the trapezoidal rule and the results are provided in Table 3. On average, a fracture energy of 92.97 J/m^2 is obtained and the standard deviation is 4.03 J/m^2. Such values are very consistent with typical fracture energies measured on mortar samples with similar water to cement ratio. Using mechanical fracture tests (Three-Point Bending on notched specimens) Haidar et al. in 2005 reported a fracture energy of 88.5 J/m^2 [24].

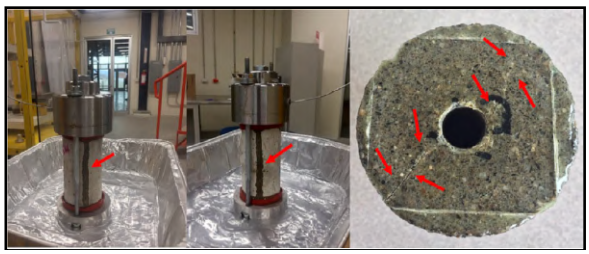

Fig. 6 Mortar specimen after hydraulic fracture test, the arrows indicate the location of through cracks.

4 FRACTURE ENERGY OF LIMESTONE AT TWO DIFFERENT TEMPERATURES

We proceed now to tests on natural rock. Limestone specimens with the same dimensions as those of mortar were prepared from rocks recovered from a geothermal reservoir in Queretaro, México. These specimens were tested at room temperature and at 100º C, this temperature being chosen since it is representative of real conditions in geothermal deposits. For the test at 100º C, the experimental set-up was placed into a Vulcan 3-400 oven regulated at constant temperature.

Note that the present experiments could be used to test hard dry rock reservoirs at higher temperatures (e.g., above 200º C). The limitation of our procedure is the flash point of the oil that is used for fracturing (232º C in our case). We should stay below this limit for safety reasons or use another fracturing fluid if high temperatures are aimed at.

Figure 7 shows the configuration used. Before starting the high-temperature tests, the specimens, saturated with oil, were mounted on the steel device inside an oven. The furnace was turned on and the temperature was raised (heating ramp at a rate of 1º C/mn) until reaching 100º C. Then, the specimen was left for 20 min more at 100º C and the tests started. In this way, the fluid contained in the specimen was at the same temperature as the rock. Regarding the fluid used for the measurement of permeability and for fracture, the pipes connected to the specimen and placed in the oven were sufficiently long to allow for heat transfer and to achieve an equilibrium between the fluid entering in the specimen and the fluid contained already in this specimen. Figure 8 and 9 shows the pressure histories for measured for the limestone specimens at both temperatures.

Overall, the curves are similar, except that the fluid flow rate has been changed from ambient temperature (0.05 mL/ min) to 100º C (0.32 mL/min) due to the decreasing viscosity of the oil with increasing temperature [25]. This

decrease of viscosity was accounted for in the calculation of the permeability. A total of eight limestone samples were used, four at room temperature and four at 100º C. The average results are summarized in Table 4 and 4.1. We may observe in this table that the permeability increases with the temperature by 44%. This is consistent with measurements reported in the literature [22].

Also, there is an increase of 20% of the fracture energy. A similar increase can be also reported for mortar samples tested according to the same procedure: from 93.42 J/m^2 at 20º C to 129.1 J/m^2 at 100º C. This growth of the fracture energy observed on mortar samples is also consistent with existing data [26].

Several explanations for this increase can be found in the literature: first of all, fracture energy increases as micro-cracking occurs due to the differences in thermal expansion of the various minerals contained in the material [27]. The principle is that, due to existing micro-cracks, a major fracture may be arrested and therefore needs more energy to propagate. It is also generally accepted that fracture is a thermally activated rate process [28]. While thermal expansion occurs, the local fracture energy decreases locally, yielding an increase of micro-cracking. Finally, thermal expansion associated with heating from room temperature to 100º C can reduce the radius of curvature at the tip of micro-cracks, thus reducing the stress intensity factor which will lead to more energy needed to propagate fracture.

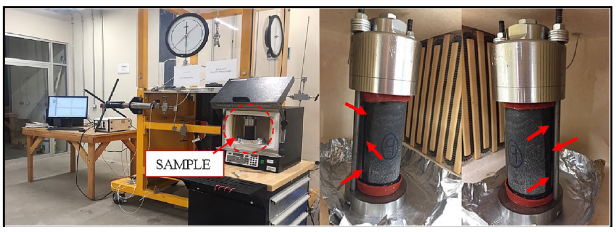

Fig.7 Set-up for high temperature tests in limestone samples. The arrows indicate the location of through cracks after the test at 100º C.

Table 4: Data for limestone at two temperatures

Quantity of samples	Temperature (ºC)	Young Modulus (GPa)	Poisson´s ratio (ν)
4	20	24.98	0.29
4	100	--	

Table 4.1: Data for limestone at two temperatures

Quantity of samples	Permeability (m^2)	Connected porosity	Fracture energy (J/m^2)
4	4.5 x 10^{-18}	0.30	213.5
4	6.5 x 10^{-18}	--	258.7

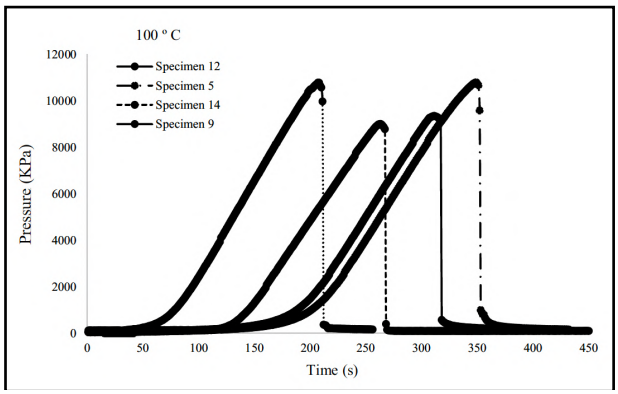

Fig.8 Pressure histories during the hydraulic fracture test for limestone at 100º C.

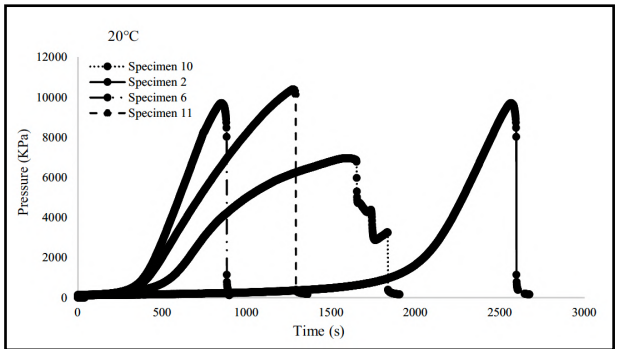

Fig.9 Pressure histories during the hydraulic fracture test for limestone at 20º C.

5 CONCLUSIONS

In this contribution, hydraulically induced fracture has been studied experimentally on mortar and rock specimens. The experiments are performed on hollow cylinders subjected to inner fluid pressure up to fracture. The fluid used is oil. The set-up allows to perform tests at room temperature, but also at temperature of 100º C at least of mortar and limestone have

been measured prior to running the fracture tests.

- The fracture energy is estimated on the basis of conservation of energy. The energy supplied by the hydraulic pump turns out to be equal to the energy dissipated during fracture. In the set-up, dissipation due to fluid viscosity is negligible. Such an estimate is directly obtained from the hydraulic fracturing test data without any specific mechanical model.

- The fracture energy estimate, applied to the present laboratory set-up, provides fracture energies of mortar at ambient temperature that are consistent with the literature data on similar materials. Temperature is found to have an influence on the fracture energy as it increases for both limestone and mortar of 20–30%.

- By looking at the variation of the fracture energy with temperature, we may speculate that in a geothermal reservoir the fractures generated will be directed towards the coldest places. Of course, such a speculation does not account for heterogeneities of rock properties or of in situ stresses. These might be much more important than the gradient of temperature and would allow for fracture propagation in hot spots of geothermal reservoirs.

- The originality of this works relies on the application of the Bernoulli's equations on an experimental set up that allows to precisely calculating the energy used for nucleations of cracks and the final fracture, regardless of the superficial area created.

This groundbreaking contribution in the field of fracture mechanics applied to geothermal deposits, built upon laboratory tests, holds promise for real-world applications. The methods proposed have undergone rigorous international scrutiny, validating their effectiveness as an additional tool to enhance permeability and improve the extraction efficiency of geothermal energy. Given that geothermal energy remains underutilized globally, despite being a green and renewable resource, contributions like this hold significant potential. The authors firmly believe that even modest efforts, such as this one, can play a role in mitigating the substantial impacts of climate change resulting from human activities.

By scanning the next QR code with your cell phone's camera or using the YouTube link, you can access a four-minute animated video on YouTube that provides a detailed explanation of this project through digital animations. The video serves the purpose of communicating our findings to a wider audience, aligning with the current trends of knowledge dissemination and social engagement.

HTTPS://N9.CL/V6TVK
(CLICK ON THE LINK)

REFERENCES

[1] Change, U. C. (2015). The paris agreement. In United Nations. Available from:https://unfcc Int /process/conferences/pastconferences/paris-climate-change-conferencenovember-2015/paris-agreement.

[2] Zalasiewicz, J., Williams, M., Steffen, W., Crutzen, P. (2010). The new world of the Anthropocene. Environ. Sci. Technol. 44 (7), pp. 2228–2231.

[3] Tester, J. W., Anderson, B. J., Batchelor, A. S., Blackwell, D. D., DiPippo, R., Drake, E. M., ... & Veatch, R. J. (2006). The future of geothermal energy. Massachusetts Institute of Technology, 358, 1-3.

[4] Yew CH, Weng X (2014) Mechanics of hydraulic fracturing. Gulf Professional Publishing, pp 1–2.

[5] Friedman M, Handin J, Alani G (1972) Fracture-surface energy of rocks. Int j Rock Mech Min Sci 9:757–766.

[6] Ouchterlony F (1988) Suggested methods for determining the fracture toughness of rock. ISRM Commission on Testing Methods. Int. j. Rock Mech Min Sci Geomech Abstr 25:71–96.

[7] Kuruppu MD, Obara Y, Ayatollahi MR, Chong KP, Funatsu T (2013) The IRSM suggested methods for rock characterization, testing and monitoring. Springer, pp 107–114.

[8] Bazant ZP, Planas J (1998) Fracture and size effect in concrete and other quasi-brittle materials. CRC Press, p 640.

[9] Bazant ZP, Kazemi MT (1990) Determination of fracture energy, process zone length and brittleness number from size effect, with application to rock and concrete. Int J Fract 44:111–131.

[10] Wei MD, Dai F, Xu NW, Zhao T, Liu Y (2017) An experimental and theoretical assessment of semi-circular bend specimens with chevron and straight-through notches for mode I fracture toughness testing of rocks. Int j Rock Mech Min Sci 99:28–38

[11] Rilem (1990) Size effect method for determining fracture energy and process zone size of concrete. Mater and Struct 23:461–465.

[12] Li W, Jin Z, Cusatis G (2019) size effect analysis for the characterization of Marcellus shale Quasi-brittle fracture properties. Rock Mech Rock Eng 52:1–18

[13] Pijaudier-Cabot G, Halimohammadi A, Nouailletas O, La Borderie C, Padin Peben A, Mathieu JP (2021) Experimental determination of the fracture energy of rocks form size effect tests on semicircular notched specimens, submitted to Rock Mechanics and Rock Engineering.

[14] Maurel O, Rees T, Matallah M, De Ferron A, Chen W, Laborderie C, Pijaudier-Cabot G, Jacques A, Rey-Bethbeder F (2010) Electrohydraulic shock wave generation as a mean to increase intrinsic permeability of mortar. Cem Concr Res 40:1631–1638

[15] Chen W, Maurel O, Reess T, Sylvestre De Ferron A, La Borderie C, Pijaudier-Cabot G, Rey-Betbeder F, Jacques A (2012) Experimental study on an alternative oil stimulation technique for tight gas reservoirs based on dynamic shock waves generated by pulsed arc electrohydraulic discharges. J Pet Eng 88–89:67–74.

[16] Mei C, Fang Q, Luo H, Yin J, Fu X (2017) A synthetic material to simulate soft rocks and its applications for model studies of socketed piles. Adv Mater Sci Eng 2017, 1565438.

[17] Gell EM, Walley SM, Braithwaite CH (2019) Review of the Validity of the Use of Artificial Specimens for Characterizing the Mechanical Properties of Rocks. Rock Mech Rock Eng 52:2949–2961.

[18] Goncalves da Silva B, Einstein H (2018) Physical processes involved in the laboratory hydraulic fracturing of granite: visual observations and interpretations. Engrg Fract Mech 191:125–142.

[19] Zhou J, Chen M, Jin Y, Zhang G (2008) Analysis of fracture propagation behavior and fracture geometry using tri-axial fracturing system in naturally fractured

reservoirs. Int j Rock Mech Min Sci 45:1143–1152.

[20] Wanniarachchi WAM, Ranjith PG, Perera MSA, Rathnaweera TD, Zhang DC, Zhang C (2018) Investigation of effects of fracturing fluid on hydraulic fracturing and fracture permeability of reservoir rocks: an experimental study using water and foam fracturing. Eng Fract Mech 194:117–135

[21] ASTM C 642–13 (2013),Standard test method for density, absorption, and voids in hardened concrete. ASTM International, West Conshohocken, PA, www. astm. org. Accessed Nov 2018.

[22] Choinska M, Khelidj A, Chatzigeorgiou G, Pijaudier-Cabot G (2007) Effects and interactions of temperature and stress-level related damage on permeability of concrete. Cem Concr Res 37:79–88.

[23] Halamickova P, Detwiler RJ, Bentz DP, Garboczi EJ (1995) Water permeability and chloride ion diffusion in Portland cement mortars: relationship to sand content and critical pore diameter. Cem Concr Res 25(4):790–802.

[24] Haidar K, Pijaudier-Cabot G, Dub. JF, Loukili A (2005) Correlation between the internal length, the fracture process zone and size effect in model materials. Mater Struct 38:201–210.

[25] Reid RC, Prausnitz JM, Poling BE (1987) The properties of gases and liquids. McGraw-Hill, New York, p 136.

[26] Menou A, Mounajed G, Carre PBH (2006) Residual Fracture Energy of Cement Paste, Mortar and Concrete Subject to High Temperature. Theoret Appl Fract Mech 45:64–71.

[27] Marinescu ID, Pruteanu M (2015) Deformation and fracture of ceramic materials. In: Doi T, Uhlmann E, Marinescu ID (eds) Handbook of ceramics grinding and polishing, 2nd edn. Elsevier Pubs, pp 50–66 (Chapter 2).

[28] Bazant ZP, Prat PC (1988) Effect of temperature and humidity on fracture energy of concrete. ACI Mater J 85:262–271.